A MARINE SEISMIC REFRACTION STUDY OF THE SANTA BARBARA CHANNEL, CALIFORNIA

GREG J. CRANDALL*, BRUCE P. LUYENDYK, MICHAEL S. REICHLE**, and WILLIAM A. PROTHERO

Marine Science Institute
and
Department of Geological Sciences, University of California, Santa Barbara, CA 93106, U.S.A.

(Accepted 20 April, 1983)

Abstract. Seismic data from a 186 km-long refraction profile in the Santa Barbara Channel have been interpreted using several velocity inversion techniques. Data were obtained during two cruises in 1978 and 1979. Seismic arrivals from fifty explosions of between 1 and 300 lbs. of TNT were recorded by two ocean bottom seismometers, four permanent ocean bottom stations (University of Southern California), and much of the United States Geological Survey/California Institute of Technology southern California seismic network. Travel-time inversion gives a V_p of 6.3 km sec^{-1} at 7.2 km depth above 7.2 km sec^{-1} at 14.4 km depth at the western end of the channel. At the eastern end, solutions suggest three sediment refractors overlying V_p of 6.4 km sec^{-1} at 7.3 km depth, above 7.0 km sec^{-1} at 11.6 km depth, above mantle arrivals with V_p of 8.3 km sec^{-1} at 21.8 km depth. The velocity structure determined by these methods suggests that the channel has a sedimentary fill of from 4 to 7 km and a layer of mafic plus ultramafic rock 14 to 17 km thick. The greatest thicknesses of sediments are restricted to east of Point Conception. The velocity data also suggest that the Franciscan formation may not be present beneath the channel. Rather, the crust here may represent a thickened portion of the Coast Range ophiolite.

1. Introduction

In an effort to better understand the tectonic and geologic history of the southern California Continental Borderland and Transverse Ranges, a refraction study of the Santa Barbara Channel was conducted during July 1978 and May 1979. This experiment consisted of a 186 km partially reversed refraction line shot along the axis of the channel. Our objectives were to determine the maximum thickness of sedimentary rock beneath the channel floor, and also to determine the depth to the mantle.

The Santa Barbara Channel (Figure 1) is a 120 km long by 40 km wide east–west trending basin. Its maximum depth is about 600 m near its center. To the north, it is bordered by the Santa Ynez Mountains, rising to over 1200 m. Its southern margin is defined by the Channel Island Platform. At its eastern end, it extends towards the Ventura Basin and associated Santa Clara Trough. To the west, the channel continues to the continental slope.

* Now at Hughes Aircraft, 4833 Fallbrook Avenue (MS, W–75) Canoga Park, CA 91304, U.S.A.
** Now at Institute of Geophysics and Planetary Physics, University of California, San Diego, CA 92093, U.S.A.

Marine Geophysical Researches **6** (1983) 15–37. 0025-3235/83/0061-0015 $03.45.

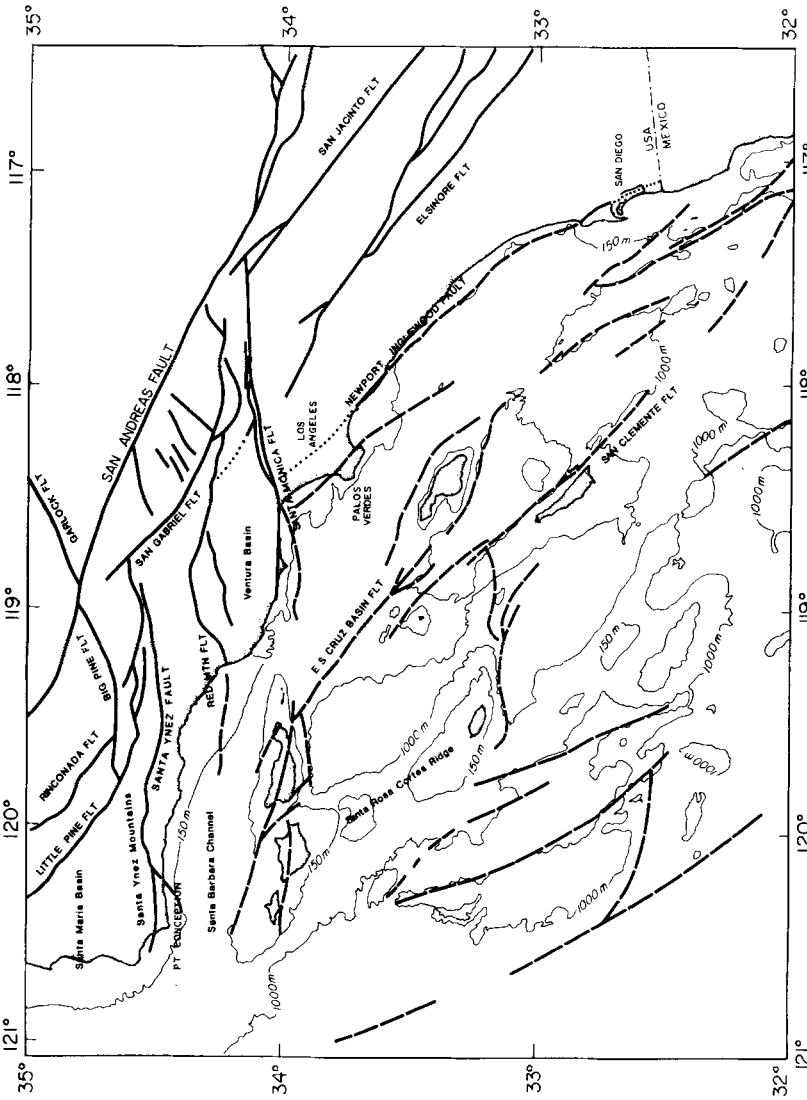

Fig. 1. Tectonic setting of the Santa Barbara Channel and the California Borderland.

Because of its geographic location, the Santa Barbara Channel plays a key role in understanding the evolution of surrounding regions. It is situated at the transition zone between the Continental Borderland and the Transverse Ranges. Its relation to either of these regions is not well understood. The Santa Barbara Channel has been described by some as the westernmost part of the Transverse Range Province (Vedder *et al.*, 1969). These two regions are very different from a tectonic and geologic standpoint. The characteristic southeast–northwest trending basin and ridge structure of the Borderland south of 34° N is in contrast to the east–west structures of the Transverse Ranges.

Sedimentation has occurred in the Santa Barbara Channel and surrounding regions since Cretaceous and probably since Jurassic time in the western Santa Ynez Mountains (Dibblee, 1950). Basement rock north of the Santa Ynez Range, which crops out along the Santa Ynez Fault (Figure 1), consists of severely deformed graywacke, shale, and chert, associated with serpentine and greenstone that are commonly assigned to the Franciscan complex (Dibblee, 1966). To the south, on Santa Cruz Island, volcanics and marine sediments are faulted against pre-Cretaceous schistose rocks which are thought to be part of the Coast Range Ophiolite (Hopson *et al.*, 1981). The location of the subsurface boundary between Franciscan basement rocks north of the Santa Ynez Range and the crystalline rocks that underlie the Channel Islands is not known (Vedder *et al.*, 1969; see also Junger, 1979).

Cretaceous and lower Tertiary strata in the channel are thought to be principally thick sub-sea fan sandstone and siltstone beds (Howell *et al.*, 1978). Deposition of nonmarine conglomerates (Sespe formation) occurred during a regional marine regression in Oligocene time. Middle Miocene volcanism occurred to the south, along the Channel Islands Platform, to the northwest (Tranquillion volcanics of Dibblee, 1950), and to the east in the Santa Monica Mountains (Shelton, 1954). Marine sedimentation occurred throughout all of the depositional basin until the Pliocene when 'north–south' compressional forces uplifted the Santa Ynez Range at the north edge along the Santa Ynez Fault, and folded and faulted the Channel Islands Platform to the south. Down-warping of the channel floor during Plio-Pleistocene time provided a site for thick sediment accumulation. Several kilometers of Plio-Pleistocene sediments have been found in the channel (Vedder *et al.*, 1969; Curran *et al.*, 1971; Howell *et al.*, 1978), including a minimum of 4 km in the northeastern channel south of the Red Mountain fault (Figure 1; Wayland *et al.*, 1978). Sedimentation has continued to the present time, with the present average rate of deposition in the central basin of about 2 mm per year (Fleischer, 1972; Hulsemann and Emery, 1961).

The major structural features in the Santa Barbara Channel and surrounding region characteristically trend east–west. East–west folds such as the Montalvo trend in the eastern channel, and left-slip faults such as the Santa Ynez fault typify the regional structure (Figure 1). Left slip faulting also occurs to the south along the Santa Cruz Island fault (Junger, 1976), as well as on the Malibu Coast fault

(Barbat, 1958) and Santa Monica fault. A recent pattern of north–south compression is indicated by reverse or thrust faults such as the Red Mountain fault at the northeast border of the channel. Howell *et al.* (1978) contend that recent episodes of deformation can be related to at least four factors: (1) regional extension (normal faulting) during late middle Miocene to late Pliocene; (2) left lateral slip at the southern boundary of the Transverse Range Province; (3) regional reverse dip-slip and north–south shortening resulting from compressional forces during late Pliocene to Holocene time; (4) Neogene clockwise rotations of at least 75° suggested by paleomagnetic vectors (Kamerling and Luyendyk, 1979).

Much multichannel seismic reflection and some refraction work has been done in the Santa Barbara Channel in conjuction with petroleum exploration, although a large part of this material is proprietary and is not available to the general public.

Yerkes *et al.* (1981) presented structure sections on the north edge of the channel constructed from multi-channel seismic reflection data and oil well logs. These sections document several kilometers of Neogene to Mesozoic sediments dipping south into the channel.

Previous work by Shor *et al.* (1976) includes a northwest trending refraction line which crossed the west end of the channel (Arguello 4 and 5), as well as a short split east–west line (Arguello 6) in the central channel (Figure 2). Although Arguello 6 was not long enough to show deep structure, or to determine mantle depth, it pointed out obvious structural differences between the Santa Barbara Channel and the rest of the Borderland, in particular a large accumulation of sediments.

2. Field Program

The Santa Barbara Channel refraction line was first shot in 1978. A second cruise in 1979 served to extend the line west in hopes of obtaining mantle arrivals and to alleviate critical gaps in the data. The line was oriented east–west along the axis of the channel and was approximately 180 km in length (Figure 2). On the first cruise, explosive sources of from 1 to 300 pounds of Dupont Tovex were used. Because of availability, TNT was used on the 1979 cruise. A total of 50 shots were fired and recorded. [Fuse lengths were timed so as to optimize the source efficiency, and to minimize the effects of the bubble pulse.] Shot depths varied between 25 to 100 m and were calculated from the bubble pulse frequency. Two ocean bottom seismometer (OBS) instruments were used; one at the east end of the line in 1978 (OBS–EXC), and one at the west end in 1979 (OBS–SAL). These instruments, developed at University of California, Santa Barbara, by W. Prothero, are microprocessor-controlled programmable digital seismometers which allow considerable flexibility in their operational mode (Prothero, 1980). During the 1978 experiment, the eastern OBS was configured as a single (vertical) channel seismometer, programmed to trigger on any seismic signal above the background noise level. Because the Santa Barbara Channel is a seismically and acoustically

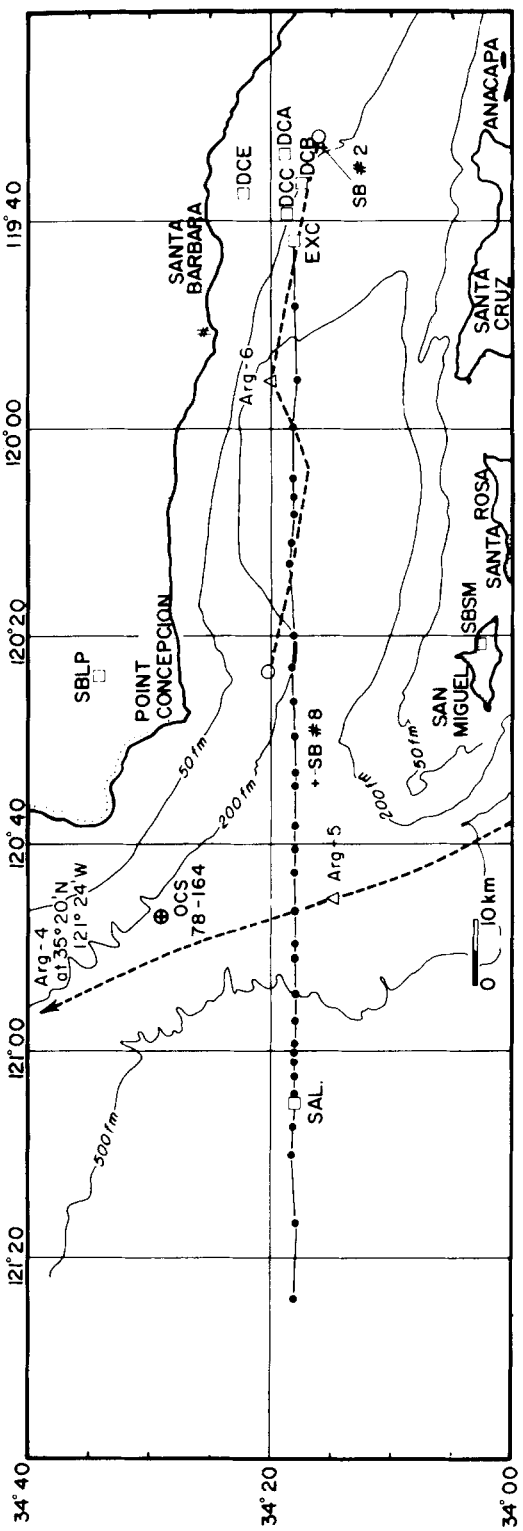

Fig. 2. Location of the seismic refraction line showing OBS locations Salsipuedes (SAL) and Excalibur (EXC), shot points (solid circles) and OBS stations of the University of Southern California (DCA, DCB, DCC, DCE). SBSM and SBLP are seismograph stations of the USGS. Arguello 4–5 is a reversed refraction profile, and Arguello 6 is a split profile completed by Shor *et al.* (1976). Sonobuoy locations (# 2, # 8) from a 1977 USGS experiment are also shown. OCS 78–164 deep test site location is also shown.

active region, background noise levels are high. Therefore, to eliminate false triggers, we decided to utilize a timed shooting window procedure on the 1979 cruise. In this mode, the instruments are programmed to record data at pre-defined times. This allowed us to detect more distant shots whose first arrivals did not trigger the OBS in 1978. In addition, in 1979 the western OBS was configured as a 3 component instrument (one vertical and two horizontal channels) in an attempt to provide shear wave (S) data in addition to compressional (P) arrivals.

Arrivals were also recorded by four permanent ocean bottom seismometers in the east end of the channel. These stations (put into operation in August, 1978 by the University of Southern California (USC) under the direction of T. Henyey) provided data to reverse the 1979 refraction line.

During a 1977 USGS experiment, two sonobuoys were deployed on the line, one over Santa Barbara basin and another west of the Oxnard shelf. These stations also provided P arrivals.

Table I gives the location of all recording stations.

TABLE I

Compilation of Station locations used in this study

OBS locations are Loran-C, corrected for local variations

Station	Lat.	Long.	Depth (m)	Comments
1. OBS SAL	34 18.31	−121 04.62	1290	May, 1979 (west)
2. Sonobuoy #8	34 16.3	−120 34.5	0	U.S.G.S. 1977
3. OBS EXC	34 18.73	−119 46.76	261	Jul, 1978 (east)
4. USC DCE	34 22.07	−119 37.31	46	May, 1979 (east)
5. Sonobuoy #2	34 15.8	−119 33.3	0	U.S.G.S. 1977

3. Data Analysis and Interpretation

3.1. Data reduction

The shot origin times were corrected for variations in shot depths and water depths by moving all shots to the seafloor. A sound velocity in water of 1463 m/sec was used. Record sections and travel time curves were then constructed for the various stations (Figures 3 and 4). Data from the horizontal components of the 3 channel OBS dropped at the west end of the channel in 1979 showed little coherent P–S conversion. Therefore only the vertical component data were used in the analysis. The USC permanent stations in the eastern channel transmit data over a radio link and telephone lines to analog recorders at USC. Large amplitude, low frequency vibrations, presumably from ocean wave noise, made these records unsuitable for plotting in record section format without hipass filtering, which was not available.

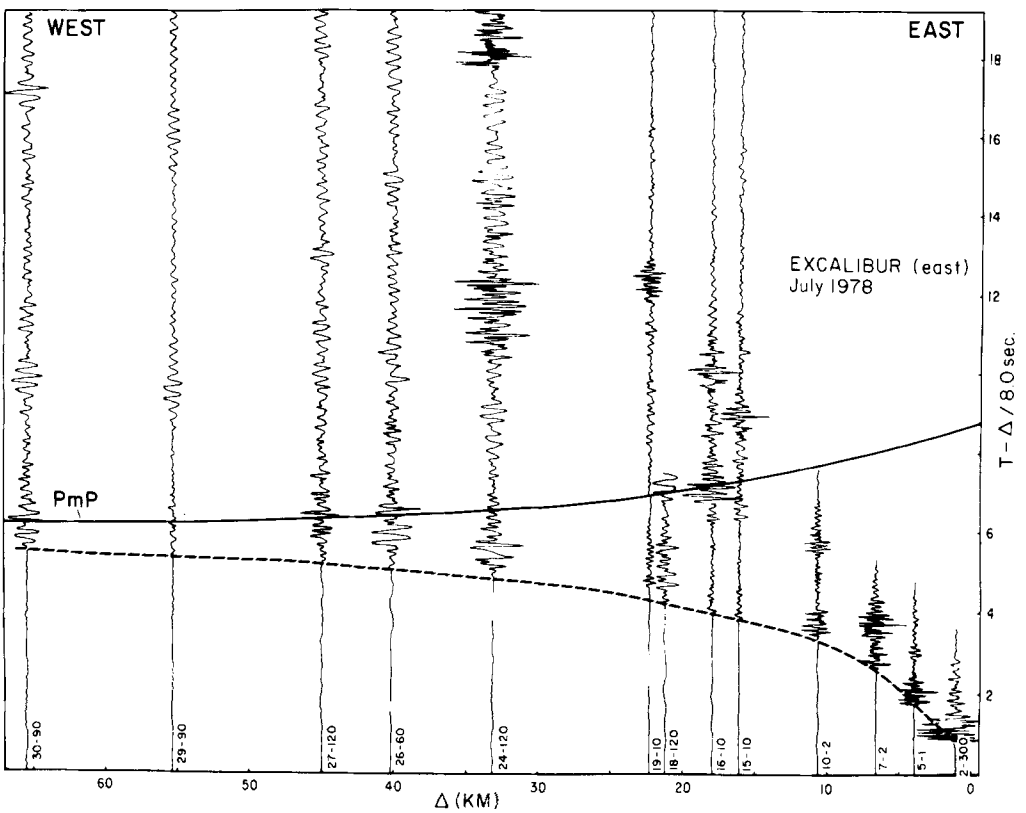

Fig. 3. Reduced travel-time record section of arrivals recorded at OBS Excalibur at the east end of the Channel. The dotted curve is the line segment interpretation. The solid curve is the theoretical arrival time of a mantle reflection (see Discussion).

First arrival times and confidence limits were estimated from the original records and plotted as travel time curves (Figure 5). Presumably because of local structural variations, travel time curves from three of the four USC stations are parallel to, but not coincident with the travel time curve for OBS–EXC. Station delays for these three stations were between 0.25 and 0.75 sec late relative to the OBS curve. The fourth USC station (DCE) had no station delay relative to the OBS. These stations are located in the east–northeast section of the channel where extensive faulting is known to exist (Figure 1). The station delays are probably the result of fault-bounded packages of low velocity sediments. Rather than introducing station corrections, we chose to use only the data from station DCE, which has no relative delay, combined with data from OBS–EXC. Recall that the data from OBS–EXC were obtained in 1978, whereas DCE data are from the following year. The lack of appreciable scatter in the combined travel time curve indicates that experimental procedures and clock corrections were adequate.

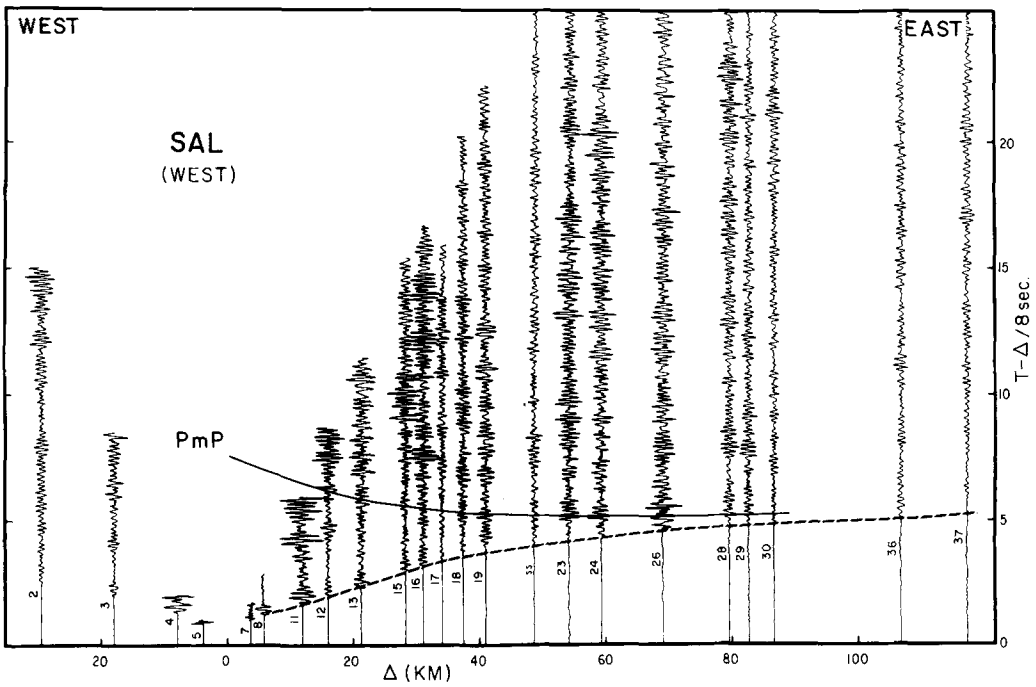

Fig. 4. Reduced travel-time record section of *P* wave arrivals recorded at Salsipuedes.

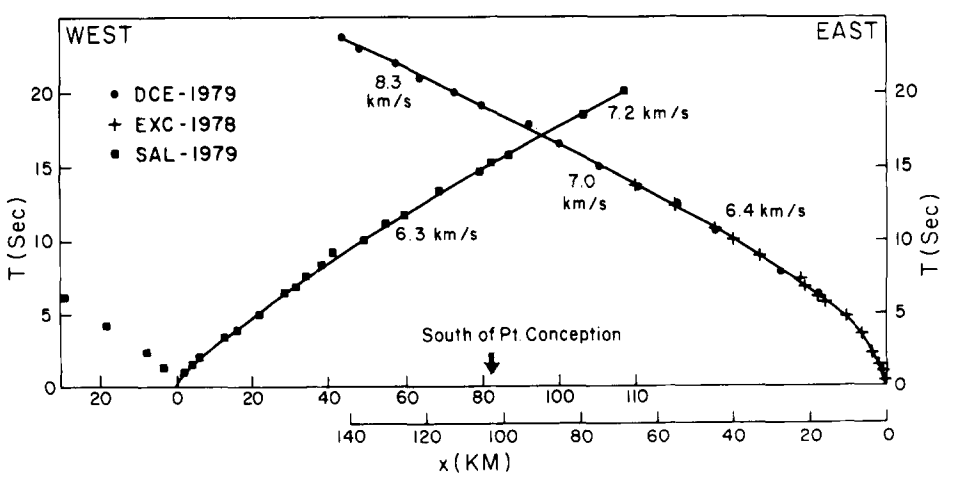

Fig. 5. Travel-time plots for first arrivals picked for OBS Salsipuedes, and for OBS Excalibur and OCE (USC).

3.2. SLOPE-INTERCEPT INTERPRETATION

The first approach we used to interpret the travel time data was a simple slope-intercept technique. Least squares, best fitting line segments were determined for the corrected travel time curves. Uniform velocity, non-dipping layer solutions were calculated (Table II; Figure 6). The non-dipping layer solution for the west end of the line (OBS–SAL) is quite similar to that of the east end (combined EXC–DCE) except for the thick accumulation of younger (?) low velocity sediments apparent in the eastern channel. Sonobuoy data obtained during a 1977 USGS cruise in the eastern channel also show these thick low velocity sediments.

Our east layer solution agrees very favorably with Shor *et al.* (1976) results for Arguello station 6 (Figure 6). We obtained a virtually identical solution down to 7 km depth. Our west solution is very different from our east solution and from the Arguello 6 split profile. The differences suggest that the upper low velocity sedimentary layers are not present west of Point Conception – that is, outside of the physiographic limits of the channel. Both of our solutions show a refractor with a V_p of about 5 km s^{-1}; however it is only about 1 km deep in the western channel versus 4 km in the east. A 6.2 to 6.4 km s^{-1} refractor appears in our solutions at a depth of about 7.2 km. The component of structural dip along the channel axis appears to be very slight because of the coincidence of the depth to this refractor at

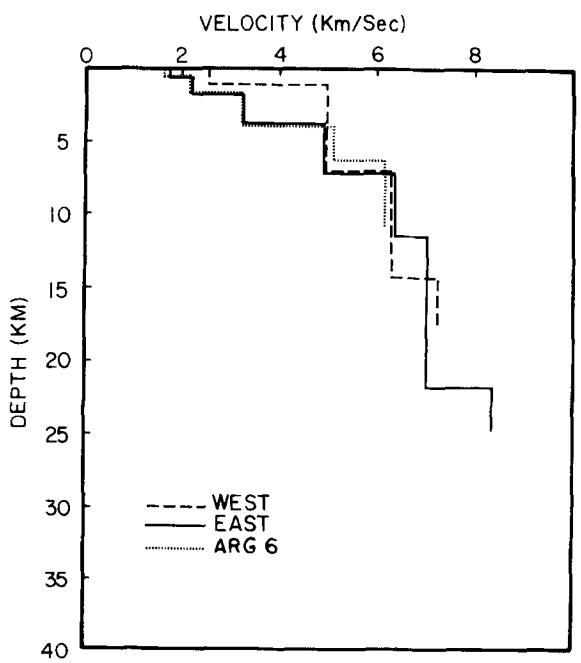

Fig. 6. A comparison of flat layer solutions (slope-intercept interpretations) for our west and east profiles, and Shor *et al.* (1976) ARG-6 solution.

either location and because the apparent velocities shooting in either direction are equal. This 6.3 km s^{-1} layer is in turn underlain by a $V_p = 7.0$ to 7.2 km s^{-1} refractor which is apparently deeper in the west. Mantle arrivals with an apparent velocity of 8.3 km s^{-1} were received at the eastern station DCE from shots at distances greater than about 95 km to the west (Figure 5). The depth to mantle, calculated by slope-intercept formulas, is approximately 22 km. Mantle arrivals of this velocity were not detected by the western OBS (SAL) because shot spacing and shot size did not result in clear first arrivals at these distances.

TABLE II

Slope-intercept (layer) solutions for stations SAL, EXC/DCE, and Sonobuoys #2 and #8

TABLE IIa. Slope-intercept solutions

Station: OBS SAL (East side of split west profile)
Direction from station to shots: West to East

Layer #	Velocity (km s^{-1})	Intercept time (sec)	Thickness (km)	Depth to top (km)
0	2.56	0.042	1.08	0
1	4.97	0.725	6.07	1.08
2	6.29	2.27	7.24	7.15
3	7.23	3.70	–	14.39
Station: OBS SAL (West side of split west profile)				
Direction from station to shots: East to West				
0	2.79	0	0.89	0
1	4.39	0.49	0.98	0.89
2	5.23	0.78	2.13	1.87
3	6.16	1.31	–	4.00

TABLE IIb

Station: EXC/DCE Combined data set
Direction from station to shots: East to West

Layer #	Velocity (km s^{-1})	Intercept time (sec)	Thickness (km)	Depth to top (km)
0	1.70[a]	0	0.66	0
1	2.19	0.49	1.18	0.66
2	3.23	1.45	1.92	1.84
3	4.90	2.57	3.55	3.76
4	6.36	3.71	4.25	7.31
5	7.01	4.43	10.32	11.56
6	8.33	6.56	–	21.90

[a]Assumed.

TABLE IIc

Station: # 2 (Sonobuoy)

Layer #	Velocity (km s^{-1})	Intercept time (sec)	Thickness (km)	Depth to top (km)
0	1.70	0	0.02	0
1	1.86	0.024	0.43	0.02
2	2.14	0.267	0.89	0.45
3	2.41	0.730	1.09	1.34
4	3.24	1.68	0.86	2.42
5	3.63	2.05	2.65	3.28
6	5.10	3.50	-	5.93
Station: # 8 (Sonobuoy)				
0	1.70	0	0.67	0
1	2.26	0.71	0.41	0.67
2	3.27	1.22	0.56	1.08
3	4.23	1.57	0.72	1.64
4	4.73	1.79	-	2.35

3.4. Travel time inversion

Simple slope-intercept layer solutions which interpret seismic refraction data in terms of a small number of planar layers of constant velocity do not extract all of the information inherent in the travel time data. This is especially true in refraction profiles having a large density of observations along the line. As pointed out by Kennett and Orcutt (1976), the numerous measurements of first arrival travel times are typically reduced to 6 to 8 parameters: the velocity and thickness of each layer.

A different approach to travel time data interpretation involves various velocity inversion methods which allow the velocity to vary continuously with depth (Bessanova *et al.*, 1974; Kennett and Orcutt, 1976; Garmany *et al.*, 1979). These methods also allow for errors in observations and give estimates of uncertainties in the velocity-depth distribution.

In our study of the Santa Barbara Channel, an extremal inversion scheme was employed. For a detailed discussion of theory and background information, see Garmany *et al.* (1979). The extremal inversion method used here is a linear programming approach developed by J. A. Orcutt at Scripps Institution of Oceanography. It produces a velocity-depth envelope which contains all possible valid solutions which fit the travel time data. Valid solutions cannot stray outside of the boundary lines which define the envelope, but not every solution contained within the envelope is valid.

The data to be inverted consisted of first arrival travel times recorded by OBS–SAL located at the west end of the channel, and arrivals to OBS–EXC and DCE at the east end of the line. The first step in the inversion method is to reparameterize the travel time data, including error estimates in time and distance,

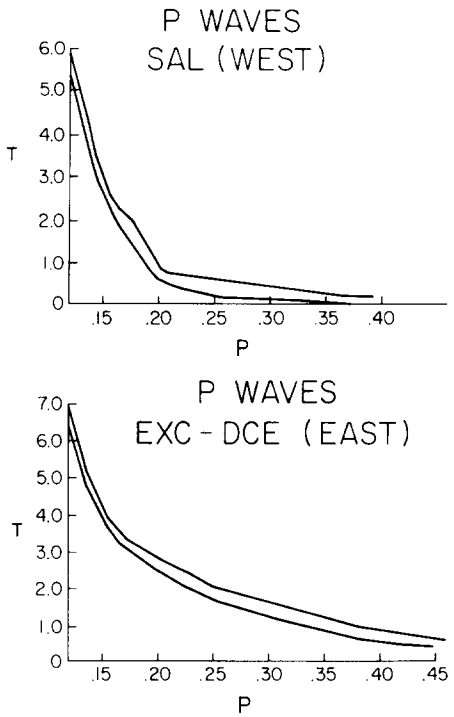

Fig. 7. Tau – P parameterization of the travel-time data for station SAL and the combined data set EXC-DCE.

into intercept time τ as a function of ray parameter P. This results in a $\tau(P)$ curve, as shown in Figure 7. The width of the $\tau(P)$ bounds depends directly upon the time and distance errors in the travel time data. Errors in first arrival times were estimated by inspecting the 'sharpness' of the arrivals on each record. In most cases, time errors were less than 0.1 sec. Navigation error was estimated at ± 0.1 km for all shots.

The data shown in the $\tau(P)$ curves were then processed with the extremal inversion program. The results (Figure 8) demonstrate that the extremal models, which contain all possible valid solutions, nicely envelope the layer solution models.

The velocity-depth distributions in Figure 8 present some interesting comparisons. Figure 9 is a combined view of the inversion solution for the east and west ends of the line. As in the layer solution model shown in Figure 6, a thick accumulation of low velocity sediments is apparent in the eastern Santa Barbara Channel. Velocity of these sediments increases with depth from about 2.2 km s^{-1} at the surface to nearly 6 km s^{-1} at a depth of about 7 km. In the west extremal solution, the low velocity sediments are confined to the upper 1 to 2 km. The velocity gradient in this upper section of the west solution is larger than any other section in either model. Beneath the upper 2 km in the western solution lies what

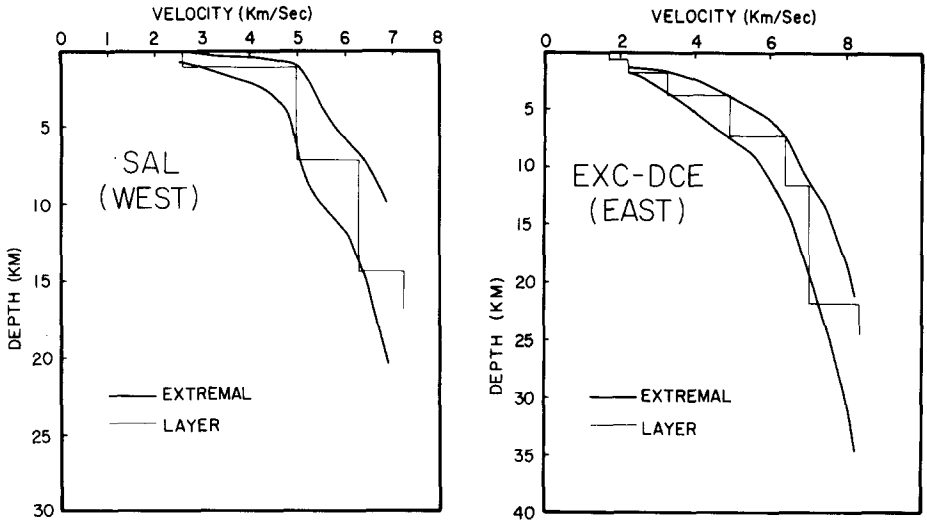

Fig. 8. A comparison of the layer solutions with extremal bound solutions for the east and west profiles.

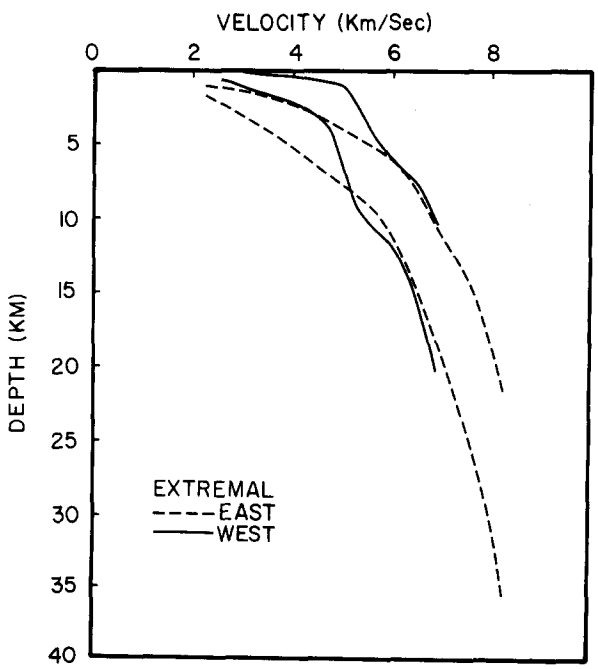

Fig. 9. A comparison of extremal bounds solutions for the east and west profiles.

might be considered a nearly uniform velocity layer. Its velocity increases only slightly from about 4.8 km s^{-1} at 2 km depth to about 5.3 km s^{-1} at 6 km. The east and west velocity-depth inversion solutions coincide at about 6 km s at a depth of around 7.5 km. This agrees well with the layer solution results which also coincide at a similar depth (Figure 8). Beneath this depth, both the east and west solutions are similar. Velocities continue to increase smoothly with depth, with the velocity at a given depth being slightly higher in the east as with the layer solution. A velocity of 8.0 km s^{-1} is observed at a depth of about 25 km in the eastern solution.

3.5. Delay time function interpretation

The similarities observed in the flat plane layer solution and inversion models along the length of the refraction line suggested that it might be possible to better define the shapes of the refractor interfaces using delay times of forward and reversed arrival. The delay time function technique (Morris *et al.*, 1969; Raitt *et al.*, 1969) as implemented by R. Detrick (Purdy and Detrick, 1978) was applied to these data. This method assumes that the configuration of the layer boundaries can be modeled as low order polynomial or Fourier functions of position. A combined data set consisting of shot and receiver locations and travel times was used to construct delay time surfaces for our selected refractors. Successively higher order polynomials were then used to represent delay time surfaces of increasing complexity. The time differences R_i, between observed travel times and solution-predicted travel times, were used to calculate the standard error about the regressions from:

$$\sigma = \sum_{i=1}^{n} [R_i^2/(N-M)]^{1/2}$$

Where N is the number of observed travel times and M is the total number of coefficients in the least squares solution (Morris, 1972; Purdy and Detrick, 1978). The quantity σ is an indicator of the overall quality of fit of a solution. Depending on the number of arrivals from a given refractor, higher order delay time solutions can become unrealistically complex, yet the standard error about the regression can remain small, thus indicating a good fit. The optimum delay time solution was generally picked as the lowest order solution in which σ had decreased and/or stabilized relative to the remaining solutions.

Figure 10 shows the delay time surfaces computed for layers 1 through 4. The $M = 3$ solution for layer 1, which corresponds to a dipping plane layer solution, gives a standard error about the regression of 0.16 sec, with residuals randomly scattered about 0 sec. The next higher ordered solution for layer 1, $M = 4$, increases the calculated velocity from 2.5 km s^{-1} to 2.6 km s^{-1}, while decreasing σ by an insignificant amount. This solution bows steeply downward in the center of the profile in an attempt to better fit the limited number of data points obtained for this shallow refraction. Higher ordered solutions are increasingly unstable in this respect. Because there were no data for this refractor near the center of the line,

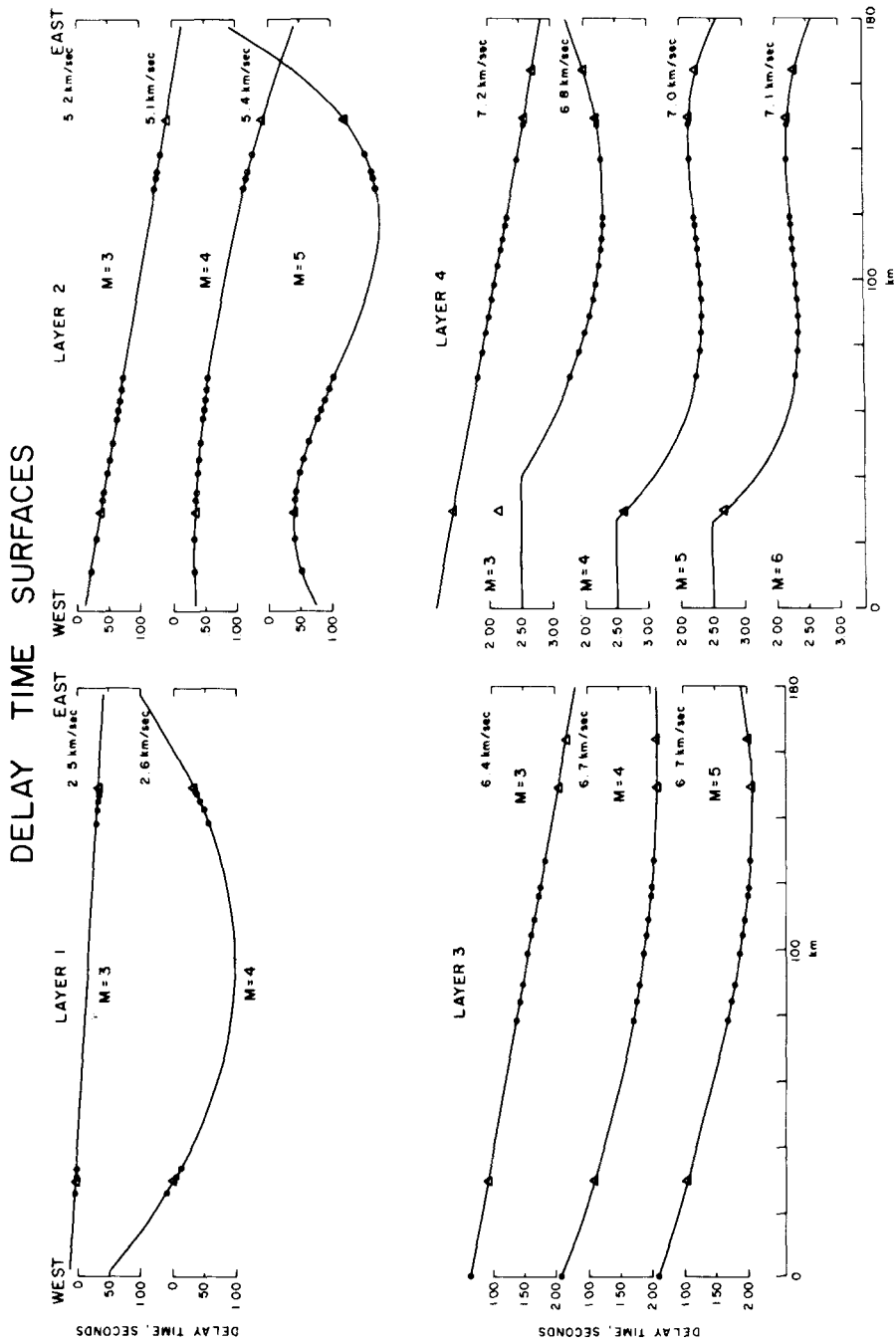

Fig. 10. Delay time profiles computed from the combined travel-time data from the east and west stations. Four layers were selected for analysis. M represents the order of polynomial required to fit the delay times (see text).

we felt it was unjustified to use the higher ordered ($M \geq 4$) solutions.

The first order solution for layer 2, $M = 3$, gives a velocity of 5.2 km s^{-1} and a standard error of 0.095 sec. Because layer 2 has numerous refracted arrivals, the $M = 4$ solution in which the standard error is reduced to 0.078 sec is preferred. The $M = 5$ delay surface reduces the standard error even more to 0.067 sec, but we do not feel that the shot and receiver coverage for arrivals from this layer is sufficient to justify the more complex solution.

Layer 3 solutions are well constrained by arrivals from the central section of the refraction line. The $M = 4$ solution improves the standard error from 0.139 to 0.089 sec, while increasing the velocity from 6.4 to 6.7 km s^{-1}. Increasing the number of terms in the polynomial to $M = 5$ causes a slight increase in the standard error ($\sigma = 0.095$ sec) while not substantially changing the shape of the delay time surface.

The standard error about the regression for layer 4 arrivals continues to decrease until the $M = 5$ solution, where it attains a minimum of $\sigma = 0.125$ sec. Higher order delay time surfaces are stable and appear to converge on the $M = 5$ configuration.

Since mantle arrivals were recorded by only one station at the east end of the line, it was not possible to construct a delay time surface for the mantle boundary.

The delay time surfaces can be converted to depths $Z_n(X)$, since the delay time to each interface is known, as well as the velocities of the overlying refractors. The depth to the nth layer is:

$$Z_n(X) = \sum_{i=1}^{n} T_i(X)\, V_i (1 - V_i^2 / V_n^2)^{-1/2}$$

where $T_i(X)$ is the delay time and V_i is the velocity of the ith layer. The structural solution obtained in this manner agrees quite closely with the structure implied by the flat lying slope-intercept solutions.

Figure 11 is a compilation of slope-intercept and delay time solutions. It represents the results of previous studies by Shor *et al.*, 1976 (Arguello 4, 5, and 6) and two USGS sonobuoys (# 2 and # 8) from a 1977 experiment, as well as the slope-intercept and delay time interpretations of our data. The similarities between the slope-intercept results and the delay time solutions are obvious to depths of about 10 km. In particular, the depth to the top of layer 1 (2.5 km s^{-1}) is very close to the slope-intercept results of sonobuoys # 2 and # 8, and the Arguello 6 model. The depth and configuration of the layer 2 (5 km s^{-1}) delay time solution closely follows the slope-intercept solutions. This refractor is deeper in the east, and bows slightly upward in the center. Some of the shallow structure depicted in the layer solutions beneath the two sonobuoys (# 2 and # 8 in Figure 11) is not resolved in the delay time solution because neither sonobuoy was included in the delay time data set. The layer 2/layer 3 interface is depicted as sloping downward in the center in the delay time solution. The 6.7 km s^{-1} velocity of layer 3 in the delay time solution is considerably higher than the 6.3 km s^{-1} apparent velocity of the

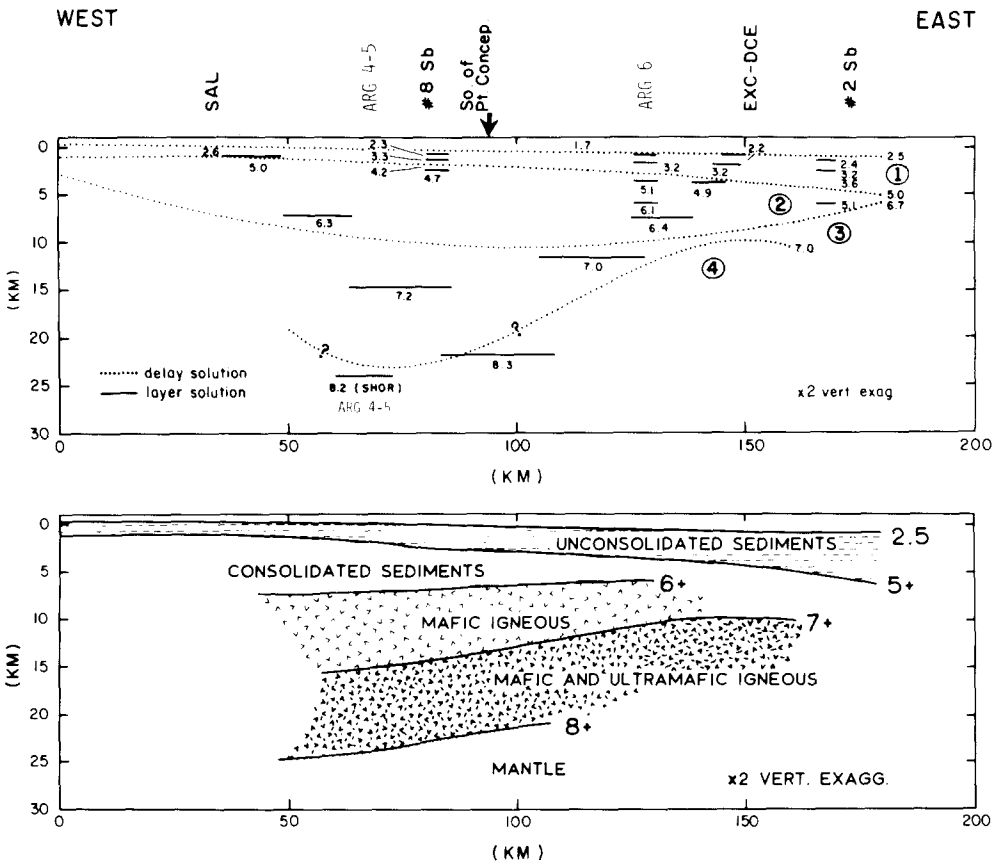

Fig. 11. (Upper) Structure section through the Santa Barbara Channel comparing delay (dotted) and flat layer (solid) solutions. All structure is calculated relative to the ocean floor. The labels # 8 and # 2 indicate the location of sonobuoys used to determine detailed V_p velocities in the upper sediments. The 8.2 km s^{-1} labelled 'SHOR' is a mantle depth determined by Shor *et al.* (1976) on station Arguello 4–5 just west of the Channel entrance (Figure 2). (Lower) Geologic interpretation of the seismic section.

OBS–SAL slope-intercept solution or the 6.4 km s^{-1} velocity of the EXC–DCE solution. The lower velocity of the slope-intercept solutions is probably a result of the structural dip indicated by the delay time model of this layer. At depths greater than 10 to 15 km, a large discrepancy is apparent in the solutions for the layer 3/layer 4 boundary. Although both the delay time solution and the individual slope-intercept solutions show this interface as dipping west as a result of layer 3 thickening to the west, the dip is much more pronounced in the delay time model. A possible resolution to this discrepancy is suggested by the extremal inversion solutions shown in Figure 9. Although the extremal bounds are quite wide, it is possible that the actual velocity profile at depths of 10 to 20 km could be better modeled as a velocity gradient, increasing with depth, rather than a 7 km s^{-1} 'layer'. If this is the case, then the delay time solution is attempting to model a layer or refractor interface which does not exist.

4. Discussion

The structural section shown in Figure 11 depicts a crustal model consisting of a low-to-medium velocity wedge, thickening towards the east, underlain by higher velocity layers which deepen and thicken in the west. The low to medium velocity section has velocities typical of saturated marine sandstones and shales (Gardner *et al.*, 1974). A well in the eastern channel just east of station DCB (Figure 1) penetrated over 4 km of Pliocene and younger silts and sands and was terminated in late Miocene sediments (Wayland *et al.*, 1978). In addition, USGS deep stratigraphic text well OCS–CAL 78–164 No. 1, located southwest of Point Conception in the western channel (Figure 2), penetrated through roughly 3 km of Neogene sandstone, siltstone, and porcelanite before reaching an apparent unconformity between Miocene and Lower Cretaceous or Uppermost Jurassic strata (Cook, 1979). The velocity-depth profile determined from a sonic log of the USGS test well is very similar to the velocity structure obtained from sonobuoy # 8. The higher velocity refractors appearing at depths greater than 7 km have velocities in excess of 6 km s^{-1}. If the 6 plus km s^{-1} layer is a sedimentary unit, then it is likely to be either a sandstone or limestone with very low or no porosity (Gregory, 1977). More probably, it represents some type of crystalline basement rock. For crystalline igneous and metamorphic rocks, velocities above 6 km s^{-1} are usually associated with mafic rocks such as basalts and gabbro. Studies on ophiolite bodies show velocities of this magnitude associated with gabbros of oceanic layer 3 (Salisbury and Christensen, 1978; Nichols *et al.*, 1980). Other refraction studies in the southern California Borderland (Shor and Raitt, 1958; Shor *et al.*, 1976) have shown basement with a velocity of between 6.5 and 7.0 km s^{-1} to be widespread throughout the Borderland. Velocities reaching 7 km s^{-1} and more usually represent crystalline rocks which include olivine or pyroxene and can be classified as ultramafic. From ophiolite studies it has been determined that cumulus olivine near the base of the gabbro units (layer 3) produces these very high velocities (Nichols *et al.*, 1980). If serpentinized ultramafic rocks are present beneath the channel it would be very difficult to detect them. Serpentinization drastically reduces V_p in ultramafic rocks and could result in a low velocity layer which might remain undetected with some refraction experiments (see Christensen, 1972 and Nichols *et al.*, 1980).

We believe that a conservative model or estimate of the gross lithology based on our refraction results would be 1 to 5 km of unconsolidated sediments over 3 to 5 km of consolidated sediments over 3 to 9 km of mafic rocks (basalt and/or gabbro) over 10 km of mafic plus ultramafic rock.

Howell and Vedder (1981) have divided the Continental Borderland into four broad northwest-trending 'terranes' – the inner, central, and outer Borderland terranes, and a fourth inside of their 'inner terrane' (see their Figure 1). The basement rocks of the inner terrane are known to be schistose rocks (Catalina Schist) intruded and overlain by Miocene plutonic and volcanic rocks. The outer

Borderland terrane has a basement composed of schistose rocks, mafic volcanic rocks, zeolite-bearing arenite and argillite, and ultramafic blocks, similar to the Coastal Belt facies of the Franciscan assemblage in northern California. Not much is known about the central terrane basement rocks, except for some mafic plutonic rocks and greenstone exposed on Santa Cruz Island. Howell and Vedder (1981) characterize the central terrane as Coast Range ophiolite overlain by Great Valley sequence Mesozoic sediments. This terrane occupies the northwest–southeast trending Santa Rosa-Cortes Ridge; they speculate that it also occupies the Santa Barbara Channel where it trends east–west. Its present orientation is possibly due to a Neogene clockwise rotation of over 90° (Crouch, 1979; Kamerling and Luyendyk, 1979; Luyendyk *et al.*, 1980). Crouch (1979) and Howell and Vedder (1981), in reviewing this area, suggest this terrane is a forearc basin environment which has been affected by crustal rotation. Therefore, geologic arguments lead to the proposition that the channel basement might be a section of Coast Range ophiolite that has been rotated into position and at a later time thickened by north–south compressional forces. The occurrence of the ophiolite on the south side of Santa Cruz Island is further supportive evidence of this interpretation (Hopson *et al.*, 1981). Outcrops of Franciscan-like rocks in the Santa Ynez Range (Dibblee, 1950) may in fact be pieces of the Coast Range ophiolite (D. G. Howell, personal communication, 1982).

The geology of the Santa Ynez Mountains and Santa Maria Basin north of the channel suggest another possibility. Basement rocks in the channel could possibly be related to the Franciscan assemblage which crops out along the Santa Ynez Fault Zone (Hall, 1981; Howell and Vedder, 1981). Composed of deformed graywacke, shale, and chert bodies intruded by serpentine and greenstone, the Franciscan assemblage has been sampled in many oil wells in the Santa Maria Basin north of the Santa Ynez River (Sylvester and Darrow, 1979). In addition, it has been suggested that the basement of the offshore area of Santa Maria consists in part of the Franciscan assemblage (Howell *et al.*, 1978). It seems unlikely, however, that the seismic velocity of the metasediments, cherts, greenstones, and serpentinites comprising the Franciscan unit would be as high as the basal refractor velocity observed in the Santa Barbara Channel. A rough estimate of the seismic velocity associated with Franciscan basement in nearby areas is from 5 to 6 km s^{-1} (B. Keller, personal communication, 1979). This velocity has been determined by the process of locating local earthquake epicenters from arrivals at stations in the Santa Ynez Mountains and the Santa Maria area. Stewart and Peselnick (1977, 1978) provide additional information regarding compressional velocities of Franciscan rocks. They studied the effects of pressure and temperature on the compressional velocity of Franciscan rocks collected in central and northern California. Their data indicate velocities from about 5.2 to 6.4 km s^{-1} for Franciscan rocks at appropriate pressure-temperature conditions (10–20 km, approximately 4 kbar, 300–400 °C). Based on these data, we conclude that Franciscan rocks do not exhibit velocities consistent with the basal refractor

velocities found in the Santa Barbara Channel.

The basement of the Santa Barbara Channel might also have been modified by crustal rifting. Crowell (1976) has reviewed the history of the Santa Clara Trough in the Ventura Basin east of the channel. There, 6.5 km of sediment were rapidly deposited in an east–west basin which began separating in mid-Miocene time, 12 to 14 my ago. By the end of Miocene time, the site of the present Santa Clara Trough was probably about 50% wider than at present. The margin of the trough opened in a wedge-shaped fashion, with the pivot point being in the east, and then closed again during Pleistocene time (Crowell, 1976). It is also possible that volcanic intrusion occurred, in the style of a nascent spreading center (Crowell, 1976; Campbell and Yerkes, 1976). The Santa Barbara Channel, which is structurally the westward continuation of the Ventura Basin, might also have gone through a similar period of crustal extension and associated volcanic intrusion, all coupled with Miocene clockwise rotation (Kamerling and Luyendyk, 1979; Luyendyk *et al.*, 1980). Seismic refraction studies in the Gulf of California, a zone of active rifting, have shown that the so-called 'main crustal layer' exhibits a seismic velocity of about 6.7 km s^{-1} (Phillips, 1964). This is identical to the velocity determined for layer 3 in our delay time solution for the Santa Barbara Channel, and might suggest a similar, intrusive origin. As Crowell (1976) points out, stretching and attenuation may be associated with thin crust. Although the crust in the Santa Barbara Channel is quite thick and the depth to mantle is about 22 km, the effects of a period of crustal extension during Miocene time might be masked by the onset of north–south shortening which began about 3 my ago (J. C. Crowell, personal communication, 1980).

In an effort to understand the nature of the crust-mantle transition beneath the channel, calculations were done to determine travel times of mantle reflections. Although the extremal boundaries of the velocity depth profiles (Figure 9) are too wide to define the crust-mantle interface, the existence of an abrupt Moho transition should be discernible on the record sections (Figures 3 and 4). An abrupt crust-mantle contact would give rise to noticeable mantle reflections (PmP). Figures 3 and 4 show the approximate position of predicted mantle reflections, assuming a mantle depth of 22 km and east and west layered velocity distributions like that in Figure 6. It is clear that large secondary arrivals exist at ranges between 50 and 80 km (Figure 4), which are very likely associated with a PmP phase. There are also large amplitude arrivals near 35–45 km (Figure 3) that might be the result of mantle reflections. However, without more dense shot spacing, it is difficult to say much about the nature of the Moho transition.

5. Concluding Remarks

The velocity structure of the Santa Barbara Channel indicates a thick sequence of low-to-medium velocity sediments overlying a high velocity basement which is probably similar to the mafic-ultramafic type basement of the Borderland to the south.

Our results indicate that 5 to 7 km of sediment fills the Santa Barbara Channel, and that the thickest accumulations are restricted to east of Point Conception. The sedimentary structure of the channel appears similar to that of the Santa Ynez Mountains to the north.

Although the mafic-ultramafic basement could be submerged Coast Range ophiolite, it is far thicker than any typical ocean crust or ophiolite section. In actuality, the crustal section might represent several layers of ocean crust, or a crust thickened by shortening. Complex internal structure caused by shortening and thickening would not be resolved by our experiment or in the older data of Shor *et al.* (1976). The sub-surface contact between this crystalline basement and the Franciscan basement of the Santa Maria Basin possibly exists as a fault or fault zone at depth along the northern border of the Santa Ynez Range.

A depth to mantle of about 22 km is not anomalously different from mantle depths in the Borderland south of the Channel Island Platform, which suggests that recent north–south compressional forces in the Santa Barbara Channel region have not significantly increased the crustal thickness or depth to mantle here compared to regions to the south.

The crust beneath the Transverse Ranges east of the Santa Barbara Channel appears thicker than that under the channel. Healy (1963) and Stierman and Ellsworth (1976) have used shots near Santa Monica and the Point Mugu earthquake of 1973 to determine estimated mantle depths of 29 to 35 km compared to our 22 km depth estimate. Crustal thicknesses in their models are about 25 to 30 km compared to our 14 to 17 km estimate; also their models have somewhat slower crustal velocities. These comparisons suggest that the eastern/central Transverse Ranges' crust is more akin to normal continental crust than to that beneath the channel. The crustal structure beneath the Santa Ynez Range, just north of the channel, is presently unknown. Preliminary interpretation of gravity data, and some seismic data, in this area, indicates that the crust is thicker under the Santa Ynez ranges than under the channel (B. Keller, personal communication, 1980).

We have employed three different methods to analyze the travel-time data. The plane layer and delay time analyses differ in their solutions for deeper velocity layers. The extremal bounds solution suggests why they differ; there are many acceptable solutions for the given data. The extremal calculation is valuable in that it allows confidence in interpretation to be established. In this regard some doubt must be expressed here as to the actual existence of a 7.0 km s^{-1} 'layer' as opposed to a gradual increase of basement velocity with depth from about 6.3 km s^{-1} at 7.2 km depth, to 8.3 km s^{-1} at 22 km depth (mantle).

Acknowledgements

We wish to thank the officers and crew of the R/V ELLEN B. SCRIPPS for their assistance during the field problem. We also appreciate the cooperation of the California Department of Fish and Game. Barry Keller and John Crowell

commented on the manuscript. This project was supported by the U.S. National Science Foundation Grant OCE77-26908. Greg Crandall also acknowledges the California Sea Grant Program for a traineeship during part of this project.

References

Barbat, W. F.: 1958, 'The Los Angeles Basin Area, California', in Weeks, L. G. (ed.), *Habitat of Oil – A Symposium: Tulsa, Okla.*, AM. Assoc. Petrol. Geol., pp. 62–77.

Bessonova, E. N., Fishman, V. M., Ryaboyi, V. Z., and Sitnitova, G. A.: 1974, 'The Tau Method for Inversion of Travel Times, I, Deep Seismic Sounding Data', *Geophys., J. Roy. Astron. Soc.* **36**, 377–398.

Campbell, R. H. and Yerkes, R.F.: 1976, 'Cenozoic Evolution of the Los Angeles Basin Area – Relation to Plate Tectonics', in Howell, D. G. (ed.), *Aspects of the Geologic History of the California Continental Borderland*, Am. Assoc. Petrol. Geol., Spec. Pub. 24, pp. 541–560.

Christensen, N. I.: 1972, 'The Abundance of Serpentinites in the Oceanic Crust', *J. Geol.* **80**, 709–719.

Cook, H. E. (ed.): 1979, 'Geologic Studies of the Point Conception Deep Stratigraphic Test Well OSC-CAL 78–164 No. 1', Outer Continental Shelf Southern California, United States: U.S. Geological Survey open file report 79–1218, p. 148.

Crouch, J. K.: 1979, 'Neogene Tectonic Evolution of the California Continental Borderland and Western Transverse Ranges', *Geological Society of America Bulletin*, Part I, Vol. 90, pp. 338–345.

Crowell, J. C.: 1976, 'Implications of Crustal Stretching and Shortening of Coastal Ventura Basin, California', in Howell, D. G. (ed.), *Aspects of the Geologic History of the California Continental Borderland*, Am. Assoc. Petrol. Geol., Spec. Pub. 24, pp. 365–382.

Curran, J. F., Hall, K. B., and Herron, R. F.: 1971, 'Geology, Oil Fields, and Future Petroleum Potential of Santa Barbara Channel Area, California', in Cram, I. H. (ed.), *Future Petroleum Provinces of the United States – Their Geology and Potential*, AM. Assoc. Petrol. Geol. No. 15, Vol. 1, pp. 192–211.

Dibblee, T. W., Jr.: 1950, *Geology of Southwestern Santa Barbara County, California; Point Arguello, Lompoc, Point Conception, Los Olivos and Gaviota Quadrangles*, Calif. Div. Mines and Geology Bull., 150, 95 p.

Dibblee, T. W., Jr.: 1966, *Geology of the Central Santa Ynez Mountains, Santa Barbara County, California*, Calif. Div. Mines and Geology Bull., 186, 99 p.

Fleischer, P.: 1972, 'Mineralogy and Sedimentation History, Santa Barbara Basin, California', *Journal of Sedimentary Petrology* **42**, 49–58.

Gardner, G. H. F., Gardner, L. W., and Gregory, A. R.: 1974, 'Formation Velocity and Density – The Diagnostic Basics for Stratigraphic Traps', *Geophysics* **39**, 770–780.

Garmany, J., Orcutt, J., and Parker, R.: 1979, 'Travel Time Inversion: A Geometrical Approach', *J. Geophys. Res.* **84**, 3615–3622.

Gregory, A. R.: 1977, 'Aspects of Rock Physics from Laboratory and Log Data that Are Important to Seismic Interpretation', in Payton, C. E. (ed.), *Seismic Stratigraphy; Applications to Hydrocarbon Exploration*, Am. Assoc. Petrol. Geol., Mem., No. 26, pp. 15–46.

Hall, C. A., Jr.: 1981, *Map of Geology along the Little Pine Fault, Parts of the Sisquoc, Foxen Canyon, Zaca Lake, Bald Mountain, Los Olivos, and Figueroa Mountain Quadrangles, Santa Barbara County, California*, U.S. Geol. Surv., Misc. Field Stud. Map, No. MF-@1285, 2 sheets, geol. map 1:24000.

Healy, J. H.: 1963, 'Crustal Structure along the Coast of California from Seismic Refraction Measurements', *J. Geophys. Res.* **68**, 5777–5787.

Hopson, C. A., Mattinson, J. M., and Pessagno, E. A., Jr.: 1981, 'Coast Range Ophiolite, Western California', in Ernst, W. G. (ed)., *The Geotectonic Development of California*, Rubey Volume I, Prentice-Hall, Englewood Cliffs, N.J., pp. 418–510.

Howell, D. G., McCulloch, D. S., and Vedder, J. G.: 1978, *General Geology, Petroleum Appraisal, and Nature of Environmental Hazards, Eastern Pacific Shelf Latitude 28° to 38° North*, Geological Survey Circular, 786, 29 p.

Howell, D. G. and Vedder, J. G.: 1981, 'Structural Implications of Statigraphic Discontinuities across the Southern California Borderland', in Ernst, W. G. (ed.), *The Geotectonic Development of*

California, Rubey Volume I, Prentice-Hall, Englewood Cliffs, N.J., United States, pp. 535–558.

Hulsemann, J. and Emery, K. O.: 1961, 'Stratification in Recent Sediments of Santa Barbara Basin as Controlled by Organisms and Water Character (California), *Journal of Geology* **69**, 279–290.

Junger, A.: 1976, 'Tectonics of the Southern California Borderland', in Howell, D. G. (ed.), *Aspects of the Geologic History of the California Continental Borderland*, Am. Assoc. Petrol. Geol., Pacific Section, Misc. Pub. 24, pp. 486–498.

Junger, A.: 1979, *Maps and Seismic Profiles Showing Geologic Structure of the Northern Channel Islands, Platform, California Continental Borderlands*, U.S. Geological Survey, Misc. Field Stud. Map, No. MF-991, 16 p.

Kamerling, M. J. and Luyendyk, B. P.: 1979, 'Tectonic Rotations of the Santa Monica Mountains Region, Western Transverse Ranges, California, Suggested by Paleomagnetic Vectors', *Geol. Soc. Am. Bull.*, Part I, **90**, 331–337.

Kennett, B. L. N. and Orcutt, J. A.: 1976, 'A Comparison of Travel Time Inversions for Marine Refraction Profiles, *J. Geophys. Res.* **81**, 4061–4070.

Luyendyk, B. P., Kamerling, M. J., and Terres, R.: 1980, 'Geometric Model for Neogene Crustal Rotations in Southern California', *Geol. Soc. Am. Bull.* **91**, 1211–1217.

Morris, G. P.: 1972, 'Delay-Time-Function Method and Its Application to the Lake Superior Refraction Data', *J. Geophys. Res.* **77**, 297.

Morris, G. B., Raitt, R. W., and Shor, G. G., Jr.: 1969, 'Velocity Anisotropy and Delay-Time Maps of the Mantle near Hawaii', *J. Geophys. Res.* **74**, 4300-4316.

Nichols, J., Warren, N., Luyendyk, B. P., and Spudich, P.: 1980, 'Seismic Velocity Structure of the Ophiolite at Point Sal, Southern California, Determined from Laboratory Measurements', *Geophys. J. Roy. Astron. Soc.* **63**, 165–185.

Phillips, R. P.: 1964, 'Seismic Refraction Studies in Gulf of California', in *Marine Geology of the Gulf of California – A Symposium*, Am. Assoc. Petrol. Geol., Mem. 3, pp. 90–121.

Prothero, W. A.: 1980, 'A Microprocessor Controlled Ocean Bottom Seismometer Capsule [abstr.]', *EOS* (Am. Geophys. Union, Trans.), **61**, No. 17, p. 308.

Purdy, G. M. and Detrick, R. S.: 1978, 'A Seismic Refraction Experiment in the Central Banda Sea', *J. Geophys. Res.* **83**, 2247.

Raitt, R. W., Shor, G. G., Jr., Francis, T. J. G., and Morris, G. B.: 1969, 'Anisotrophy of the Pacific Upper Mantle', *J. Geophys. Res.* **74**, 3095–3109.

Salisbury, M. H. and Christensen, N. I.: 1978, 'The Seismic Velocity Structure of a Traverse through the Bay of Islands Ophiolite Complex, Newfoundland, An Exposure of Oceanic Crust and Upper Mantle', *J. Geophys. Res.* **83**, 805–817.

Shelton, J. S.: 1954, 'Miocene Volcanism in Coastal Southern California', in *Geology of Southern California*, Calif. Div. of Mines Bull. 170, pp. 31–36.

Shor, G. G., Jr., Raitt, R. W., and McGowan, D.: 1976, *Seismic Refraction Studies in the Southern California Borderland* 1949–1974, Scripps Inst. Oceanog. Ref. 76–13.

Shor, G. G., Jr. and Raitt, R. W.: 1958, *Seismic Studies in the Southern California Continental Borderland*, Scripps Inst. Oceanog. Ref. 58–78, 17 p.

Stewart, R. and Peselnick, J.: 1977, 'Velocity of Compressional Waves in Dry Franciscan Rocks to 8 kbar and 300 °C', *J. Geophys. Res.* **82**, 2027–2039.

Stewart, R. and Peselnick, J.: 1978, 'Systematic Behavior of Compressional Velocity in Franciscan Rocks at High Pressure and Temperature', *J. Geophys. Res.* **83**, 831–839.

Stierman, D. J. and Ellsworth, W. L.: 1976, 'Aftershocks of the February 21, 1973 Point Mugu, California Earthquake', *Seismol. Soc. Am. Bull.* **66**, 1931–1952.

Sylvester, A. G. and Darrow, A. C.: 1979, 'Structure and Neotectonics of the Western Santa Ynez Fault System in Southern California, *Tectonophysics* **52**, 389–405.

Vedder, J. G., Wagner, H. C., and Schoellhamer, J. E.: 1969, 'Geological Framework of the Santa Barbara Channel Region', in *Geology, Petroleum Development and Seismicity of the Santa Barbara Channel Region, California*, U.S. Geological Survey Professional Paper 679-A, pp. 1–11.

Wayland, R. G., Acuff, A. D., McCulloh, T. H., Raleigh, C. B., Vedder, J. G., and Yenne, K. A.: 1978, *Facts Relating to Well No. 5, Pitas Point Unit Area, and the Earthquake of August* 13, 1978, *Santa Barbara Channel, California*, U.S. Geological Survey Open File Report 78–906, 67 p.

Yerkes, R. F., Greene, H. G., Tinsley, J. C., and Lajoie, K. R.: 1981, *Maps Showing Seismotectonic Setting of the Santa Barbara Channel Area, California*, U.S. Geol. Surv., Misc. Field Stud. Map, No. MF–1169, 25 p., geotect. maps 1:250000.